

## Immune landscape of isocitrate dehydrogenase-stratified primary and recurrent human gliomas

Pravesh Gupta<sup>†,1,✉</sup>, Minghao Dang<sup>†</sup>, Shivangi Oberai, Simona Migliozi, Rakesh Trivedi<sup>1,✉</sup>, Gayatri Kumar<sup>1,✉</sup>, Mekenzie Peshoff, Nancy Milam, Aml Ahmed, Krishna Bojja, Tuan M. Tran, Joy Gumin, Carlos Kamiya-Matsuoka, Jason Huse<sup>✉</sup>, Kathryn Cox, Jianzhuo Li, Huma Shehwana<sup>✉</sup>, Sameer A. Sheth, Rodriguez Saxon, Sun Baohua, Brittany Parker Kerrigan, Atul Maheshwari, Edwin Roger Parra Cuentas, Nicholas E. Navin, Amy B. Heimberger, Frederick F. Lang<sup>✉</sup>, Antonio Iavarone<sup>✉</sup>, Karen Clise-Dwyer, Linghua Wang<sup>✉</sup>, and Krishna P. Bhat<sup>1,✉</sup>

All author affiliations are listed at the end of the article

<sup>1</sup>Present affiliation: Department of Cancer Biology, Mayo Clinic, Phoenix, Arizona, 85259, USA.

<sup>†</sup>These authors equally contributed to the manuscript.

Corresponding Authors: Pravesh Gupta, PhD, Department of Translational Molecular Pathology, The University of Texas MD Anderson Cancer Center, Houston, TX, 77030, USA ([pravesh001@e.ntu.edu.sg](mailto:pravesh001@e.ntu.edu.sg)); Linghua Wang, PhD, Department of Genomic Medicine, The University of Texas MD Anderson Cancer Center, Houston, TX, 77030, USA ([lwang22@mdanderson.org](mailto:lwang22@mdanderson.org)); Krishna P. Bhat, PhD, Department of Translational Molecular Pathology, The University of Texas MD Anderson Cancer Center, Houston, TX, 77030, USA ([bhat.krishna@mayo.edu](mailto:bhat.krishna@mayo.edu)).

For the podcast associated with this article, please visit '<https://soc-neuro-onc.libsyn.com/the-immune-landscape-of-idh-mutant-and-idhwt-glioma>'

### Abstract

**Background.** Human gliomas are classified using isocitrate dehydrogenase (IDH) status as a prognosticator; however, the influence of genetic differences and treatment effects on ensuing immunity remains unclear.

**Methods.** In this study, we used sequential single-cell transcriptomics on 144 678 and spectral cytometry on over 2 million immune cells encompassing 48 human gliomas to decipher their immune landscape.

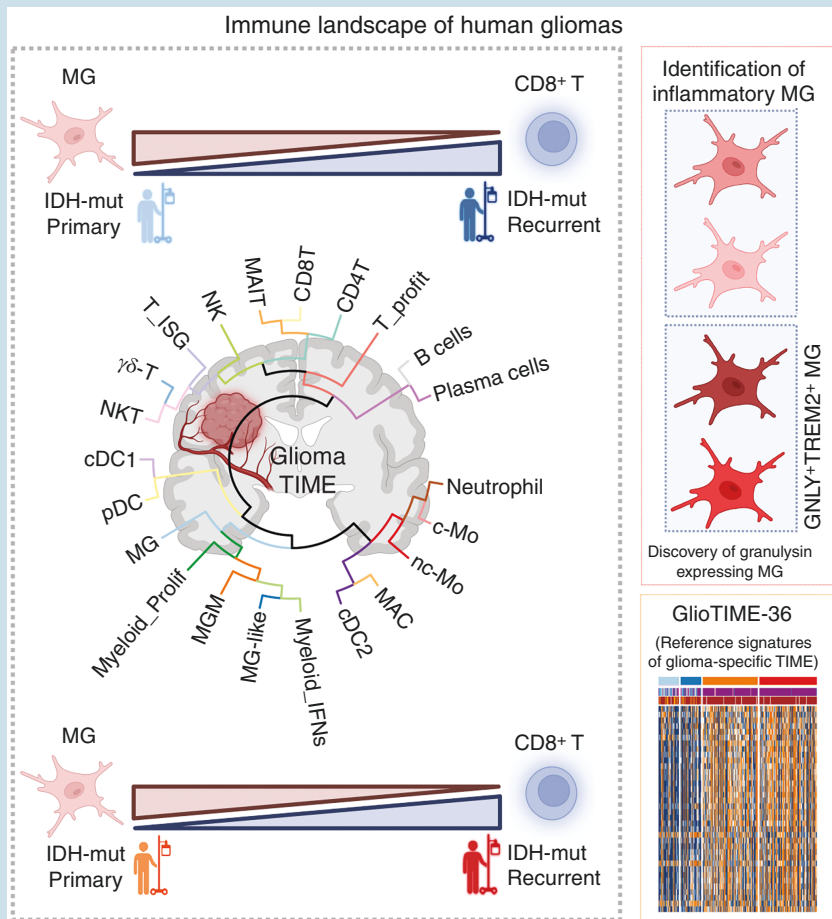
**Results.** We identified 22 distinct immune cell types that contribute to glioma immunity. Specifically, brain-resident microglia (MG) were reduced with a concomitant increase in CD8<sup>+</sup>T lymphocytes during glioma recurrence independent of IDH status. In contrast, IDH-wild type-associated patterns, such as an abundance of antigen-presenting cell-like MG and cytotoxic CD8<sup>+</sup>T cells, were observed. Beyond elucidating the differences in IDH, relapse, and treatment-associated immunity, we discovered novel inflammatory MG subpopulations expressing granulysin, a cytotoxic peptide that is otherwise expressed in lymphocytes only. Furthermore, we provide a robust genomic framework for defining macrophage polarization beyond M1/M2 paradigm and reference signatures of glioma-specific tumor immune microenvironment (termed GlioTIME-36) for deconvoluting transcriptomic datasets.

**Conclusions.** This study provides advanced optics of the human pan-glioma immune contexture as a valuable guide for translational and clinical applications.

### Key Points

- Twenty two distinct immune cell types contribute to glioma immunity.
- IDH-wt gliomas show predominance of inflammatory microglial subpopulations expressing granulysin.
- We provide glioma-specific reference signatures (GlioTIME-36) as a valuable tool for immunogenomic deconvolution.

### Graphical Abstract



### Importance of the Study

Gliomas are the most common and aggressive neoplasms of the CNS and harbor both brain-resident and infiltrating immune cells that can modulate tumor growth. Therefore, a detailed understanding of the tumor immune microenvironment of glioma is necessary to develop tumor-specific immunotherapy. Here, we provide a side-by-side comparison of the immune contexture across primary and recurrent gliomas stratified by isocitrate dehydrogenase (IDH)

status. Our comprehensive multiomics interrogation of IDH-classified brain tumors sculpts a glioma-specific immune atlas, leading to the identification of novel inflammatory microglia (MG) and rare immune subpopulations. Additionally, we demonstrate the utility of this single-cell atlas in resolving MG/macrophage polarization states and immunogenomic deconvolution of transcriptomic data from the human glioma GLASS cohort.

In brain pathologies such as traumatic injury or neurodegenerative disorders, phagocytic cells comprising microglia (MG), CNS-associated monocytes (Mo), and macrophages (MAC) are the first responders to resolve the underlying inflammation.<sup>1</sup> For instance, in Alzheimer's disease, MG prevent disease progression by clearing amyloid plaques.<sup>2</sup> In contrast, tumor-associated macrophages

(TAMs) are linked to poor prognosis of brain neoplasms such as gliomas.<sup>3</sup> Although primarily phagocytic in nature, myeloid cells are plastic and can undergo functional diversification under the influence of dysregulated cytokine and chemokine milieu contributed by infiltrating bone marrow-derived leukocytes and tumor cells.<sup>4,5</sup> Myeloid cell functions can also be differentially influenced by tumor

necrosis and inflammation, a defining feature of isocitrate dehydrogenase-wild type (IDH-wt) when compared to that of isocitrate dehydrogenase-mutant (IDH-mut) gliomas.<sup>6</sup> Standard-of-care treatments such as surgical resection followed by temozolamide and ionizing radiation can unintentionally disrupt anatomical barriers and cause immunomodulation and necrosis,<sup>7–10</sup> all of which can skew the properties of myeloid cells and other leukocytes.

Studies on glioma-specific tumor immune microenvironment (TIME) studies are focused mostly on MG/MAC that are collectively referred to as glioma-associated MAC, myeloid-derived suppressor cells, and tumor-infiltrating lymphocytes.<sup>11–15</sup> However, simple dichotomization of MAC polarization into M1/M2 functional phenotypes ignores their heterogeneity and plasticity.<sup>16–18</sup> Independent single-cell transcriptomics and cytometry investigations<sup>10,12,14,19–24</sup> have advanced our understanding of the brain TIME. However, these studies were largely restricted to analyses of glioblastoma (GBM, a high grade glioma)<sup>12,14,19,23</sup> or associated myeloid cells,<sup>14,19,22</sup> and lacked in-depth characterization of IDH-mut low-grade gliomas,<sup>13,25</sup> specifically under relapsed settings. Given that most clinical trials prioritize patients with recurrent glioma,<sup>26</sup> comparative studies of the brain TIME for discerning immune alterations associated with IDH status, disease relapse, and treatment-induced changes are imperative, and will unlock avenues for optimally designing immunotherapies.

To address these gaps, we performed single-cell RNA-sequencing (scRNA-seq), bulk mRNA-sequencing (RNA-seq), and spectral cytometry analyses of tumor-associated leukocytes to define the TIME of IDH-stratified primary and standard-of-care-treated patients with recurrent glioma. Here, we present a systematic overview of the myeloid and lymphoid cell states and highlight their differential infiltration and immune reactivity patterns linked to IDH status, tumor relapse, and inflammation severity. In addition, we demonstrate the direct application of our detailed immune atlas for understanding the heterogeneity of spectral polarization of MAC at a relatively high resolution and for defining reference signatures of leukocyte genes for immunogenomic deconvolution.

## Materials and Methods

### Collection of Tissues From Human Brain Tumor Samples (Hereafter Referred to as Tissue)

Tissue samples were collected from 56 patients with glioma undergoing neurosurgery, after obtaining informed consent (approved by the Internal Review Board [IRB] of MD Anderson Cancer (MDACC) protocol numbers LAB03-0687, LAB04-0001, and 2012-0441 (see detailed clinical information in *Supplementary Table 1*). Five quasi-normal tissue samples were collected from patients undergoing neurosurgery for epilepsy (approved by the IRB of Baylor College of Medicine, protocol number H-13798). All experiments complied with the guidelines of the IRB of MDACC. Detailed materials and methods are available in *Supplementary Materials*.

## Results

### Transcriptionally Defined Leukocyte Diversity in IDH-Stratified Primary and Recurrent Human Gliomas

We performed scRNA-seq on flow cytometry-sorted CD45<sup>+</sup> leukocytes obtained from the tumors of 18 IDH-stratified patients, comprising IDH-mut primary (IMP), IDH-mut recurrent (IMR), IDH-wt primary (IWP), and IDH-wt recurrent (IWR) gliomas (hereafter referred to as glioma subtypes). Three quasi-normal and non-glioma brains (NGBs) from an adjacent dysembryoplastic neuroepithelial tumor or a refractory epileptic non-neoplastic patient were used as controls (*Figure 1A; Supplementary Table 1*). Using a previously described protocol for immune cell enrichment<sup>27</sup> and CD45<sup>+</sup> sorting, we consistently obtained highly pure CD45<sup>hi</sup>/CD45<sup>lo</sup> leukocyte subpopulations in gliomas and NGBs (*Supplementary Figure 1A–C*) unlike those observed in previous studies,<sup>28–30</sup> which may be owing to the differences in tissue dissociation protocols.

We applied the Harmony algorithm for correcting batch effects and calculated the Local Inverse Simpson's Index (LISI) to assess the extent of integration of cell types. The LISI scores and statistical assessment of the overall dataset revealed efficient mixing of cell types across batches (*Supplementary Figure 1D–H*) and statistical analysis of the overall dataset revealed minimal batch effects (*Supplementary Figure 1H*). Potential doublets/multiplets, cell debris, and low-quality cells were removed using a multistep approach. Unsupervised clustering analyses resolved 144 678 leukocytes into myeloid (*n* = 100 587) and lymphoid cells (*n* = 44 091) within and across glioma subtypes, and confirmed that the glioma TIME was myeloid-dominant, which was consistent with previous reports<sup>10,12–14,20–24</sup> with the exception of IWR gliomas that had similar proportions of myeloid and lymphoid cell populations (*Figure 1B*). A negligible number of neuronal-lineage cells (*n* = 284) were excluded from subsequent analyses (data not shown). Glioma-associated myeloid cell populations exhibited a phenotypic continuum characterized by overlapping gene features between MG and MAC subsets (eg, expression of *SPP1*, *APOE*, and *C1QC*); however, it was resolved by core MG gene sets, including *CX3CR1*, *GPR34*, *P2RY12*, *P2RY13*, *SALL1*, *TAL1*, and *TMEM119* (*Figure 1C; Supplementary Figure 1I and J*). Dendritic cells (DCs), Mo, and neutrophils were identified based on the expression of canonical gene signatures (*Figure 1C; Supplementary Figure 1I and J; Supplementary Table 2*).

Microglia represented the largest myeloid cell type among the NGB and IMP glioma subtypes (*Figure 1C*). In contrast, concomitant with MG attrition, invading MG-like cells co-expressing the signature genes of MG (*SORL1*, *SAMD9L*, and *GPR34*) and MAC (*GLDN*, *MSR1*, and *CD163*), *VCAN<sup>+</sup>FCN1<sup>+</sup>* classical Mo (c-Mo), *TCF7L2<sup>+</sup>FCGR3A<sup>+</sup>* nonclassical Mo (nc-Mo), *CD163<sup>+</sup>MARCO<sup>+</sup>* *FN1<sup>+</sup>* MAC, and *TMEM176A<sup>+</sup>SELENOP<sup>+</sup>* MDM proportionately increased in IMR, IWP, and IWR glioma subtypes (*Figure 1C; Supplementary Figure 1J; Supplementary Table 2*).

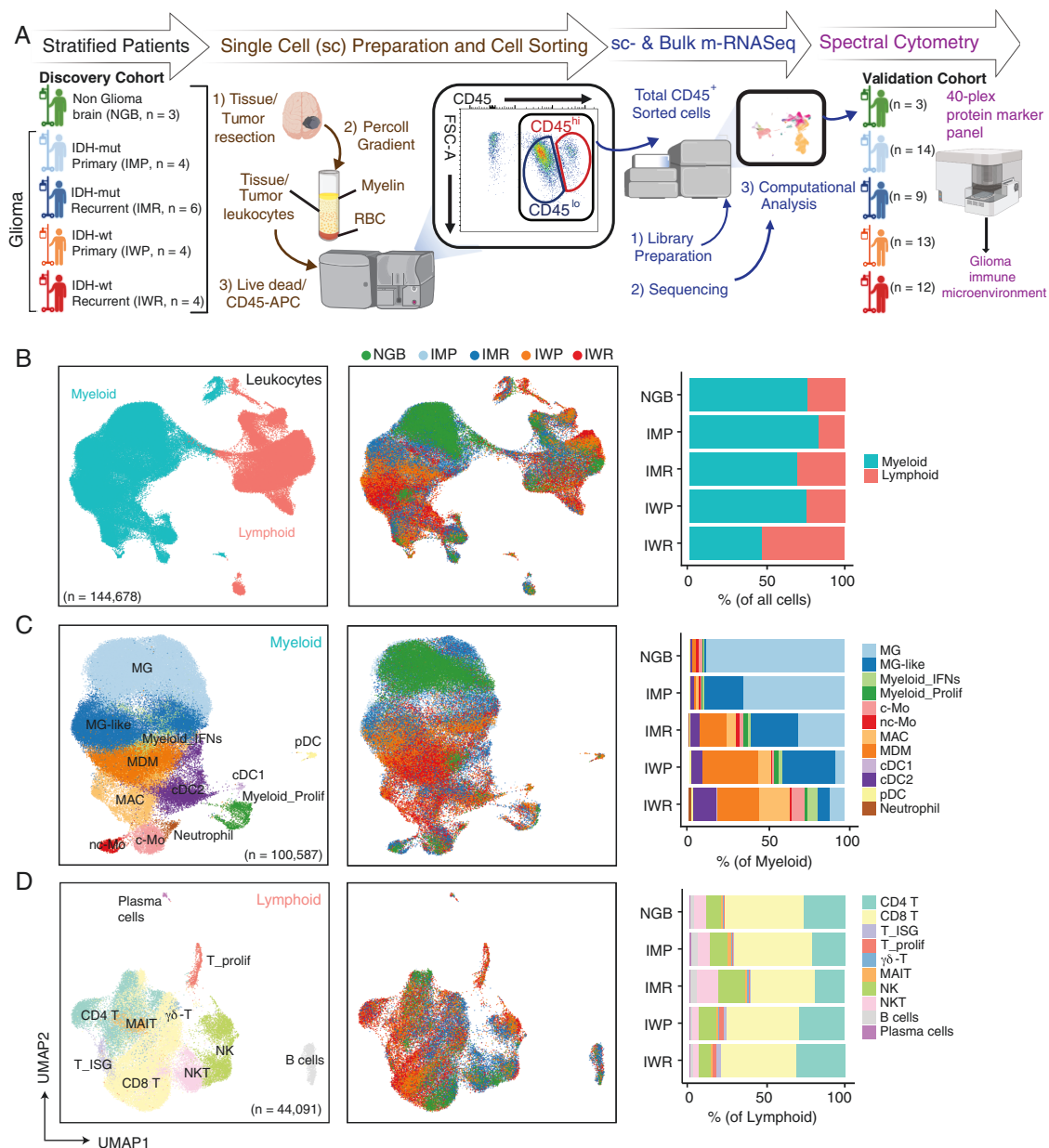


**Figure 1.** Single-cell transcriptional landscape of the glioma TIME. (A) A scheme depicting the experimental workflow spanning sample preparation of resected brain tissues/tumors, scRNA-seq, spectral flow cytometry validation, and computational analysis. For scRNA-seq analyses, patients were stratified as the NGB ( $n = 3$ ), IMP ( $n = 4$ ), IMR ( $n = 6$ ), IWP ( $n = 4$ ), and IWR ( $n = 4$ ) groups as a discovery patient cohort (hereafter collectively referred as glioma subtypes) (see details in Supplementary Table 1). The dissociated and CD45-APC-stained cells were sorted to obtain pure CD45<sup>+</sup> tumor-associated leukocytes. Subsequently, matched scRNA-seq and bulk RNA-seq were performed followed by computational analysis. Cell types defined by scRNA-seq were further validated by a 40-plex protein marker spectral flow cytometry panel in an extended validation patient cohort comprising NGB ( $n = 3$ ), IMP ( $n = 14$ ), IMR ( $n = 9$ ), IWP ( $n = 13$ ), and IWR ( $n = 12$ ). (B–D) UMAP visualization of unsupervised clustering analysis of leukocytes ( $n = 144\,678$ ) that passed quality filtering as shown in (B) all immune cells; (C) myeloid lineage clusters ( $n = 100\,587$ ) identified as microglia (MG), microglial-like cells (MG-like), interferon gene module-associated myeloid cells (Myeloid\_IFNs), proliferative myeloid cells (Myeloid\_Prolif), classical monocytes (c-Mo), nonclassical monocytes (nc-Mo), macrophages (MAC), monocyte-derived MAC (MDM), conventional dendritic cell 1 (cDC1), conventional dendritic cell 2 (cDC2), plasmacytoid DC (pDC), and neutrophil; (D) lymphoid lineage clusters ( $n = 44\,091$ ) identified as CD4 T, CD8 T, interferon-stimulated gene associated T (T\_ISG), proliferative T (T\_Prolif), gamma-delta T ( $\gamma\delta$ -T) lymphocytes, mucosal-associated invariant T (MAIT) cells, natural killer (NK), natural killer T (NKT), B lymphocytes (B cells), and plasma cells. Cells are color-coded for their inferred cell types (left) and the glioma subtypes of their corresponding tumors (middle). Stacked bar plots (right) show the percentage cell composition of each glioma subtype.

Increased proportions of professional antigen-presenting cells (APCs) such as *CLEC9A*<sup>+</sup> cDC1, *CD1C*<sup>+</sup> cDC2, and *IL3RA*<sup>+</sup> plasmacytoid DC (pDC) were observed in IWR gliomas compared to those in other glioma subtypes. Other notable glioma-associated myeloid cells included MAC/MG\_IFNs with interferon (IFN)-stimulated genes (*IFI44L*, *IFI6*, and *ISG15*), Myeloid\_Proliferative cells (*MKI67* and *PCLAF*), and *JMJD1C*<sup>+</sup> neutrophils (Figure 1C and Supplementary Figure 1J). Based on previous studies<sup>31–34</sup> that the attrition of tissue-resident macrophages is accompanied by concomitant infiltration of monocytic derivatives in inflammatory conditions, we speculate that infiltration of non-MG myeloid cells is a consequence of depleting niches of MG in gliomas.

Inter- and intra-tumoral glioma-associated lymphoid cell types resolved into T lymphocytes, *TRDC*<sup>+</sup> γδ-T cells, *SLC4A10*<sup>+</sup> MAIT cells, *NKG7*<sup>+</sup>*KLRF1*<sup>+</sup> natural killer (NK) cells, *CD3D*<sup>+</sup>*NKG7*<sup>+</sup> NK T (NKT) cells, *CD79A*<sup>+</sup>*MS4A1*<sup>+</sup> B lymphocytes, and *MZB1*<sup>+</sup>*IGHG1*<sup>+</sup> plasma cells (Figure 1D; Supplementary Figure 1K and L; Supplementary Table 3). Notably, among glioma-infiltrating lymphoid lineage cells, we identified rare cell types such as MAIT and NKT, which have not been previously reported.<sup>15,35</sup> Overall, we report 12 myeloid and 10 lymphoid cell types (Supplementary Figure 1M; Supplementary Table 4) with transcriptionally defined phylogenetic cellular relationships in the TIME of IDH-stratified primary and recurrent human gliomas (Supplementary Figure 1N). Tissue-resident signatures (*CCR7*, *S100A9*, *PLAUR*, *ITGAE*, and *CD69*) suggested an infiltrative rather than intravascular nature of glioma-associated leukocytes (Supplementary Figure 1O), which was further corroborated by canonical gene expression in major cell types across different anatomical regions of tumors through bulk RNA-seq data of Ivy GBM Atlas Project (Supplementary Figure 1P). Furthermore, Co-detection by Indexing (CODEX) protein assay confirmed the presence of major cell types such as DCs, MAC/Mo, and T cells in the tumor and perivascular regions (Supplementary Figure 1Q).

### Immunophenotyping of Human Gliomas by Spectral Cytometry

A 40-parameter (Supplementary Table 5A) spectral cytometry-based immunophenotyping assay (detailed gating strategies in Supplementary Figure 2A and B) was performed on 48 tumors ( $n = 9 - 13/\text{glioma subtype}$ ) and 3 refractory epileptic non-neoplastic brain samples (clinical characteristics summarized in Supplementary Table 1) to understand the differences in composition of immune cells between primary and recurrent IDH-wt and IDH-mut gliomas. As IDH-wt and IDH-mut gliomas are biologically distinct and non-overlapping pathogenic phenotypes, statistical comparisons are largely restricted to treatment naive (IMP and IWP) and glioma relapse (IMR and IWR) within molecular subtypes to infer TIME differences during disease progression. Unlike previous reports,<sup>21,24</sup> relatively low or comparable proportions of neutrophils were observed across glioma subtypes (Supplementary Figure 2C), probably owing to the differences in protocols for leukocyte enrichment. Because CD11c expression defines DCs and tissue-resident MAC such as MG,<sup>36,37</sup> P2RY12 expression

was used as an MG restrictive marker to distinguish between MG and CD11c<sup>+</sup> DC phenotypes. Accordingly, we differentiated reactive CD11c<sup>+</sup> MG from CD11c<sup>-</sup>CCR2<sup>-</sup> resting MG (Supplementary Figure 2B). P2RY12<sup>+</sup>CX3CR1<sup>+</sup> MG were the most abundant cells across glioma subtypes with the highest proportions evident in NGB, IMP, and IWP groups (Figure 2A and D). Not only did the proportion of P2RY12<sup>+</sup>CX3CR1<sup>+</sup> MG, but also CD11c<sup>+</sup> reactive MG were significantly reduced with glioma recurrence (IMR and IWR) compared to treatment naive (IMP and IWP) subtypes (Figure 2A and D), while resting MG was observed across gliomas and NGB, and were abundant in the IWR group (Figure 2D; Supplementary Figure 2D). The bone marrow-derived myeloid compartment herein referred as non-MG myeloid cells comprising CD11c<sup>+</sup>CCR2<sup>+</sup> Mo-MG, CD68<sup>+</sup>CCR2<sup>-</sup> MAC, CD68<sup>+</sup>CCR2<sup>+</sup> MDM, CD14<sup>+</sup>CD16<sup>-</sup> c-Mo, CD16<sup>+</sup>CD14<sup>-</sup> nc-Mo, Clec9A<sup>+</sup> cDC1, and CD1c<sup>+</sup> cDC2 cells did not show any significant differences among inter-glioma subtypes (Supplementary Figure 2D–G). Amongst lymphoid lineage cells, T cells including CD8<sup>+</sup> T cells, but not CD4<sup>+</sup> T and Foxp3<sup>+</sup> regulatory T cells (Tregs) exhibited significantly increased infiltration during glioma recurrence compared to those by treatment-naive gliomas, which was independent of IDH status (Figure 2B and D; Supplementary Figure 2H and I). NK cells and their subpopulations comprising CD56<sup>hi</sup>, CD56<sup>lo</sup>, and CD16<sup>+</sup> NK cells did not show any apparent inter-glioma differences; however, their abundance significantly increased in IWR glioma subtype when compared to that in NGB (Figure 2C; Supplementary Figure 2J). Nonclassical subpopulations of T cells included NKT, γδ-T and T cell receptor (TCR) Va7.2<sup>+</sup> MAIT cells and did not show any noticeable differences across glioma subtypes (Supplementary Figure 2K). Taken together, we confirmed the presence of all major cell types and their enrichment patterns across glioma subtypes (Figure 2D; Supplementary Figure 2L; Supplementary Table 5B). Overall, we observed a negative correlation in the frequencies between MG and CD8<sup>+</sup> T lymphocytes in gliomas (Figure 2E), which was relatively more prominent in IMR glioma subtype (Supplementary Figure 2M). Among glioma subtypes, an inverse correlation was observed between the frequencies of MG and MAC in treatment-naive gliomas (Supplementary Figure 2M).

### Identification of Inflammatory and APC-Like Microglia in Human Gliomas

In humans, microglial states associated with the CNS have been defined in Alzheimer's disease,<sup>38</sup> multiple sclerosis,<sup>37</sup> epilepsy,<sup>39</sup> and to a limited extent in primary IDH-wt and IDH-mut gliomas using single-cell transcriptomics.<sup>12,14,19,22,23,25</sup> In our study, MG were distinguished from MAC using core gene sets of MG including lineage-specific transcription factors, *TAL1* and *SALL1* (Supplementary Figure 1J and S3A). A subclustering analysis was performed to further classify MG and MG-like cells into 9 cell states with distinct expression profiles (Figure 3A; Supplementary Figure 3B and C; Supplementary Table 6). The MG cell states were annotated using gene ontology (GO) analysis as a guide to infer functional likelihoods such as antigen-presentation associated gene

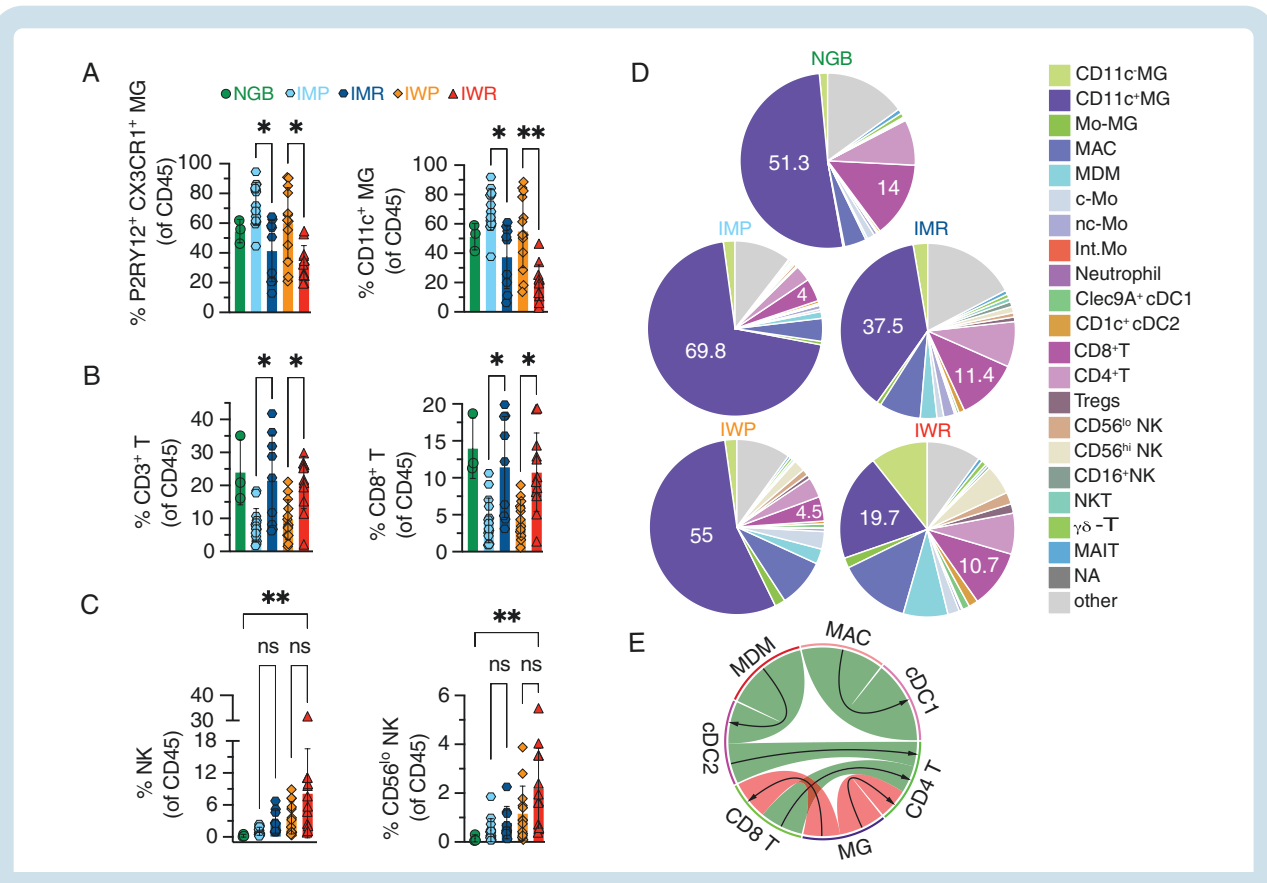


**Figure 2.** Immune contexture of human gliomas validated by spectral flow cytometry. Color-coded scatter bar plots represent the relative proportions and error bars represent an interval of maximum and minimum values  $\pm$  standard deviation (SD) of the indicated immune cell types (of CD45<sup>+</sup> leukocytes) across glioma subtypes: NGB ( $n = 3$ ), IMP ( $n = 14$ ), IMR ( $n = 9$ ), IWP ( $n = 13$ ), and IWR ( $n = 12$ ). (A) P2RY12<sup>+</sup>CX3CR1<sup>+</sup> MG (left), CD11c<sup>+</sup> MG (right). (B) T lymphocytes (gated on CD3<sup>+</sup> TCR-γδ<sup>+</sup>TCRV-α7.2<sup>-</sup>) (left), CD8<sup>+</sup> T cell (gated on T) (right). (C) NK cells (gated on CD56<sup>+</sup>) (left), CD56<sup>lo</sup> NK (right). Statistical significance in A–C was determined by using the Kruskal–Wallis test at \* $P < .05$ , \*\* $P < .01$  between NGB and glioma subtypes: IMP versus IMR, IWP versus IWR, and IMP versus IWP; n.s. = not significant. (D) Pie chart summarizing the proportion of indicated immune cell types in NGB and across glioma subtypes in TIME. (E) Circos plots showing the multiple correlation matrix between frequencies of leukocytes in human gliomas.  $P < .05$ .  $R > 0.6$  is represented in red, and  $R < -0.6$  is shown in green.

modules (eg, *CSTD* and *MS4A4A*) in MG\_APc-like 1 and MG\_APc-like 2 clusters, and a lipid metabolism-associated *LPL*<sup>+</sup> MG\_Lipid Metab cluster. IDH-mut glioma-associated MG clusters included *BAG3*<sup>+</sup> MG\_hsp and *ATF* expressing metabolically enriched MG\_OxPhos. Across glioma subtypes, a *CCL4L2* expressing inflammatory MG\_Inflam 1 cluster associated with response to tumor necrosis factor, interleukin-1 and lipopolysaccharide GO terms and a granulysin (*GNLY*) expressing (*GNLY*<sup>+</sup>*TNF*<sup>+</sup>) cluster defined as MG\_Inflam 2 were observed (Figure 3A; Supplementary Figure 3D; Supplementary Table 7). Moreover, 2 novel inflammatory MG states (*GNLY*<sup>+</sup>*TREM2*<sup>+</sup>*TMIGD3*<sup>+</sup> MG\_IFN and *GNLY*<sup>+</sup>*TREM2*<sup>+</sup>*IL1A*<sup>+</sup> MG\_Inflam 3) characterized by expression of *GNLY* and Triggering receptor expressed on myeloid cell 2 (*TREM2*), and an inflammatory lysozyme (*LYZ*) expressing MAC state (*CD163*<sup>+</sup>*LYZ*<sup>+</sup> MAC\_IFN) (Figure 3B; Supplementary Figure 3E; Supplementary Table 8) were resolved from the Myeloid\_IFN cluster (Figure 1C). Four inflammatory MG phenotypes with shared and distinct gene signatures were identified. These included proinflammatory

transcription factors (*CEBPD*, *ATF3*, and *FOS*) enriched in MG\_Inflam 1 and 2, inflammasomes (*NLRP3*, *IL1A*, and *IL1B*) enriched in MG\_Inflam 1-3, and the interferon pathway (*IFI6*, *IFIT1*, and *ISG15*) enriched in MG\_Inflam 3 and MG\_IFN (Figure 3B). *GNLY* expression in MG was corroborated with the results of a previous study,<sup>14</sup> in which such inflammatory signature was restricted to MG-TAMs among myeloid cells in newly diagnosed and recurrent GBM patients (Figure 3C). The CODEX assay confirmed co-expression of *GNLY* and *TREM2* in a subpopulation of MG corroborating the presence of *GNLY*<sup>+</sup>*TREM2*<sup>+</sup> MG clusters (Figure 3D). Overall, we identified transcriptionally heterogeneous MG with inherent functional likelihoods across glioma subtypes. Comparative analyses of glioma-associated MG subpopulations with previously reported GBM-associated MG clusters<sup>12,14,19</sup> showed resemblances to APC-like, homeostatic, and lipid metabolism cluster from this study. Notably, we identified novel MG subtypes such as metabolic MG\_OxPhos and stress-responsive MG\_hsp (Supplementary Figure 3F), probably owing to the inclusion of IDH-mut gliomas in this study.

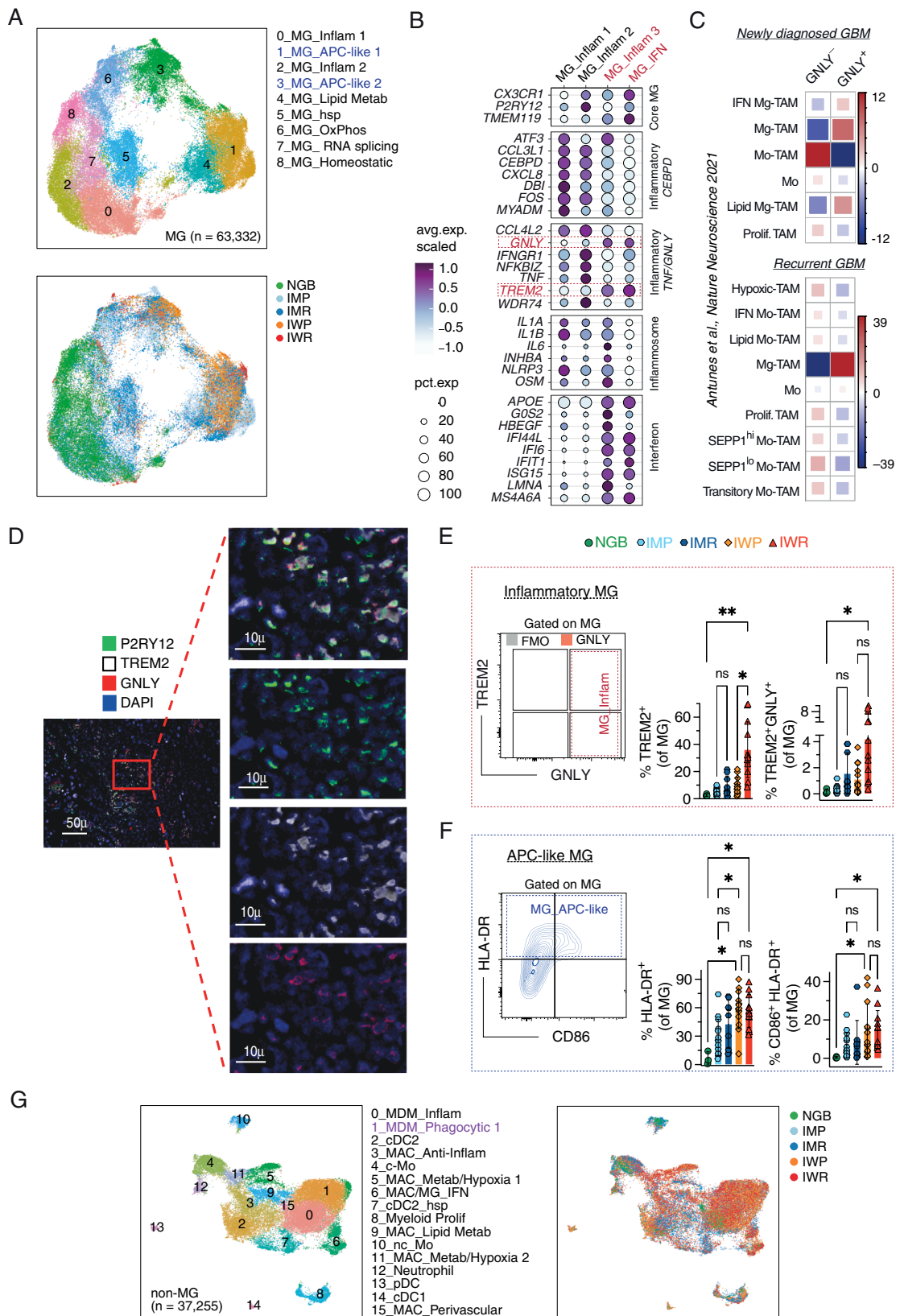
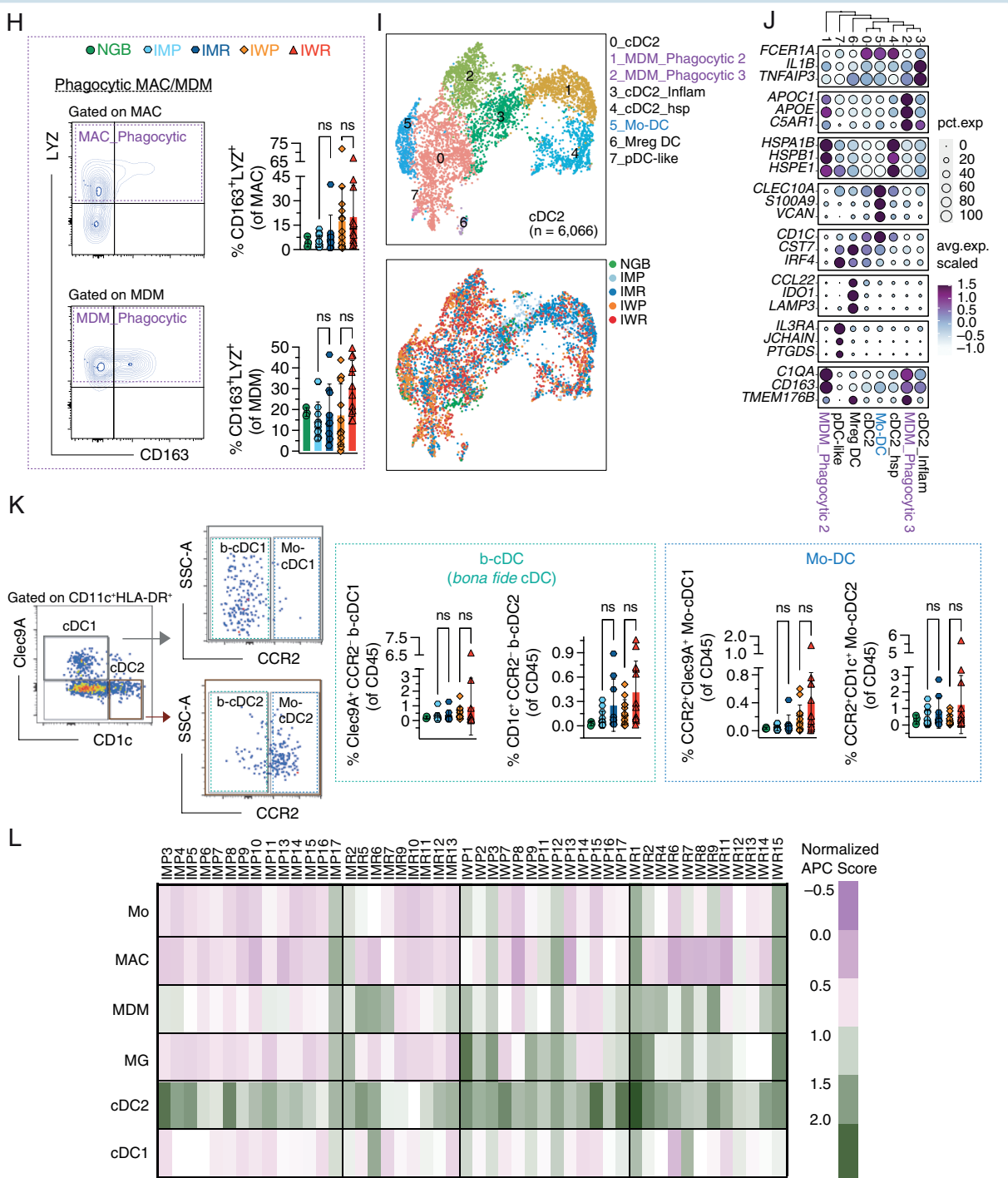


**Figure 3.** Heterogeneity of MG, non-MG myeloid cells, DCs, and their functional states in the glioma TIME. (A) UMAP visualization of unsupervised clustering analysis of MG cell states ( $n = 63\,332$ ). Cells are color-coded for their inferred MG cell states (top) and their distribution across glioma subtypes (bottom). (B) Bubble plot showing the scaled expression (indicated by the color of the circle) and percentage of expression (indicated by the size of the circle) of selected inflammatory marker genes from the top 50 differentially expressed genes (DEGs) of inflammatory MG clusters. NGB ( $n = 3$ ), IMP



( $n = 4$ ), IMR ( $n = 6$ ), IWP ( $n = 4$ ), and IWR ( $n = 4$ ). (C) Plot showing  $P$ -value and color-coded chi-squared test-derived standardized residuals as index of the statistical significance and strength of the association between GNLY gene expression and myeloid cell types from Antunes et al. (2021) in primary (top) and recurrent GBM (bottom). Red and blue indicate positive and negative enrichment for expression of GNLY in each myeloid cell type.  $P < 2.2e-16$ ,  $\chi^2$  test. (D) Representative example of multiplex tissue images from brain tumor samples of GBM. Composite and unmixed images ( $20\times$  and  $40\times$  magnification, scale bars represent 50 and 10  $\mu\text{m}$ , respectively) showing a panoramic view of P2RY12 (green), GNLY (red), and TREM2 (white) and DAPI (4',6-diamidino-2-phenylindole) and high magnification showing cells co-expressing P2RY12, GNLY, and TREM2 and DAPI and individual marker expression. (E) Flow cytometry (FCM) dot plot showing the expression of TREM2 and GNLY on MG (in red), and GNLY fluorescence minus one (FMO) control (gray) (left). Corresponding color-coded scatter bar plots showing proportions of TREM2 $^+$  and inflammatory TREM2 $^+$ GNLY $^+$  cells (right). (F) FCM contour plot showing the expression of CD86 and HLA-DR on MG (left). Corresponding color-coded scatter bar plots showing proportions of HLA-DR $^+$  and CD86 $^+$  HLA-DR $^+$  cells (right). (G) UMAP visualization of unsupervised clustering analysis of non-MG myeloid cell states ( $n = 37$  255). Cells are color-coded for their inferred cell states (top), and their distribution across glioma subtypes (bottom). (H) FCM contour plot showing the expression of LYZ and CD163 on MAC (top, left) and MDM (bottom, left). Color-coded scatter bar plots depicting the proportions of MAC (top, right) and MDM (bottom, right) expressing CD163 $^+$ LYZ $^+$ . (I) UMAP visualization of unsupervised clustering analysis of cDC2 cells ( $n = 6066$ ). Cells are color-coded for their inferred cell states (left).

and their distribution across glioma subtypes (right). (J) Bubble plot showing the scaled expression (indicated by the color of the circle) and percentage of expression (indicated by the size of the circle) of selected cluster-specific genes from the top 50 DEGs of cDC2-associated clusters. (K) FCM pseudo-color plots showing the expression of CD1c and Clec9A (gated on CD11c<sup>+</sup> HLA-DR<sup>+</sup> cells, left). FCM pseudo-color plots showing the expression of CCR2 on Mo-cDC1 and Mo-cDC2 cells (middle). Corresponding color-coded scatter bar plots showing the proportions of *bona fide* Clec9A<sup>+</sup>CCR2<sup>-</sup> b-cDC1 and CD1c<sup>+</sup>CCR2<sup>-</sup> b-cDC2, and monocytic derivatives CCR2<sup>+</sup>Clec9A<sup>+</sup> Mo-cDC1 and CCR2<sup>+</sup>CD1c<sup>+</sup> Mo-cDC2 subsets (right). b-cDC and Mo-cDCs were gated on CD11c<sup>+</sup> and Clec9A<sup>+</sup> cells. (L) Heatmaps obtained from normalized APC score derived from median fluorescence intensities (MFIs) of B2M, HLA-DR, CD86, and LYZ in indicated myeloid cell types. Statistical significance in D, E, G, and J was determined by using the Kruskal-Wallis test at \*P < .05, \*\*P < .01 between NGB and glioma subtypes, IMP versus IWP, IWP versus IWR, and IMP versus IWP; n.s. = not significant. Glioma subtypes used for spectral cytometry analysis: NGB (n = 3), IMP (n = 14), IMR (n = 9), IWP (n = 13), and IWR (n = 12).

The finding that GNLY was expressed in MG was intriguing because this cytolytic molecule is generally associated with NK and CD8<sup>+</sup> T cells, and has not been previously reported in MG<sup>12,14,19</sup> (Supplementary Figure 3E and F). The occurrence of GNLY<sup>+</sup> TREM2<sup>+</sup> MG subpopulation was also confirmed by spectral cytometry across gliomas, predominantly in the IWR subtype compared to that in NGB. Interestingly, the GNLY<sup>+</sup> MG subpopulation mostly expressed TREM2 (Figure 3E; Supplementary Figure 3G). Phagocytic MG characterized by the expression of scavenger receptor (CD163) and lysozyme (LYZ) showed higher proportions of LYZ<sup>+</sup> and LYZ<sup>+</sup>CD163<sup>+</sup> MG in IDH-wt gliomas than those in NGB (Supplementary Figure 3H). Additionally, we detected MG-APC-like cells using HLA-DR, a canonical marker of antigen presentation and CD86, a co-stimulatory molecule. Higher proportions of HLA-DR<sup>+</sup> and CD86<sup>+</sup> HLA-DR<sup>+</sup> MG were observed in IDH-wt gliomas than those in NGB (Figure 3F; Supplementary Figure 3G). Additionally, we observed a remarkable abundance of Ki-67<sup>+</sup> proliferative MG, in IWP compared to that in IMP glioma subtypes (Supplementary Figure 3I).

### Diversity of Infiltrating Non-MG Myeloid Cells and APCs in Human Gliomas

To understand the diversity of non-MG myeloid cells, a subject of immense interest in IDH-wt gliomas,<sup>10,12,14,19,21,23,24</sup> we analyzed infiltrating non-MG myeloid subpopulations across IDH-classified gliomas and identified 16 non-MG myeloid cell states including 6 MAC and 2 MDM clusters (Figure 3G; Supplementary Figure 3J; Supplementary Table 9). Based on DEGs and GO analyses, MAC were annotated as *IL10*<sup>+</sup> MAC\_Anti-Inflam, and multiple metabolic MAC clusters, including MAC\_Metab/Hypoxia 1, MAC\_Metab/Hypoxia 2, and *LIPA*<sup>+</sup> MAC\_Lipid Metab subpopulations, were enriched with genes related to hypoxia (eg, *SDS* and *HMOX1*). A cluster of *LYVE1*<sup>+</sup> MAC, which was associated with vasculature and defined as MAC\_Perivascular was also observed. Among the MDMs, *C1QA*<sup>+</sup> MDM\_Phagocytic 1 was associated with receptor-mediated endocytosis and *JUN*<sup>+</sup>*SELENOP*<sup>+</sup> MDM\_Inflam was associated with positive regulation of inflammation (Figure 3G; Supplementary Figure 3J and K; Supplementary Tables 9 and 10). This is consistent with a previous study that identified *SELENOP*<sup>+</sup> MDM/Mo-TAMs.<sup>14</sup> In fact, a comparison of monocytic and MAC/MDM clusters showed cluster-specific similarities, for example, MAC\_Lipid Metab, MAC\_Metab/Hypoxia, and MG/MAC\_IFN (Supplementary Figure 3L

and M).<sup>12,14</sup> Comparable proportions of phagocytosis-competent<sup>40</sup> MAC and MDM were observed, as assessed by LYZ and CD163 expression (Figure 3H; Supplementary Figure 3N); however, the proliferation of MAC was higher in IWP than in IMP glioma subtype (Supplementary Figure 3O). Monocytic infiltrates in glioma TIME included *FCN1*<sup>+</sup>*CD14*<sup>+</sup> c-Mo and *FCGR3A*<sup>+</sup>*TCF7L2*<sup>+</sup> nc-Mo and did not show any noticeable differences across other glioma subtypes (Supplementary Figures 2F and 3J). We observed comparable infiltration of DCs, including *CLEC9A*<sup>+</sup> cDC1 and *CD1C*<sup>+</sup> cDC2 across gliomas, in contrast to negligible DC infiltration in NGB, which may be a consequence of tumor-associated inflammation (Supplementary Figures 2G and 3J).

Although glioma-associated heterogeneity of DCs has been recently described,<sup>12,14</sup> given the strength of our study that included approximately 6000 DCs, we sought to provide a coherent picture of these APCs in the glioma TIME. Consistent with previous reports,<sup>12,14,41,42</sup> where cDC2 has been described as a heterogeneous group of cells, we further subclustered cDC2 in our cohort (Figure 3I). This analysis revealed *CD1C*<sup>+</sup>*FCER1A*<sup>+</sup> classical cDC2, *IL1B*<sup>+</sup> cDC2\_inflam, and a heat shock protein-associated cluster *HSPA1A*<sup>+</sup> cDC2\_hsp. The remaining cDC2-like clusters had high expression of monocytic (*VCAN* and *S100A9*) and MAC-associated genes (*C1QA*, *CD163*, and *TMEM176B*), which were defined as MDMs (MDM\_Phagocytic 2 and MDM\_Phagocytic 3). Other cDC2-like cells showed strong expression of *LAMP3* and *IDO1* and were defined as Mreg DCs,<sup>14</sup> and a pDC-like cluster (*IL3RA* and *PTGDS*) (Figure 3I and J; Supplementary Table 11). Previously defined Mo-DC clusters,<sup>12,14</sup> had a higher degree of similarity to the MDM clusters described in our study (Supplementary Figure 3P). The transcriptionally defined *CLEC10A*<sup>+</sup>*VCAN*<sup>+</sup> Mo-DC cluster was further examined with spectral cytometry in an extended cohort. Indeed, we observed that CCR2<sup>+</sup> Mo-DCs, which can be classified into CCR2<sup>+</sup>*CLEC9A*<sup>+</sup> Mo-cDC1 and CCR2<sup>+</sup>*CD1c*<sup>+</sup> Mo-cDC2 subsets did not show any statistical differences across gliomas. The proportions of *bona fide* DCs (b-DCs), such as CCR2-*CD1c*<sup>+</sup> b-cDC2 and CCR2-*Clec9A*<sup>+</sup> b-cDC1 showed a similar distribution across gliomas (Figure 3K). Similar proportions of activated cDC1 and cDC2 (both *bona fide* and Mo-DC derivatives) were noticed across gliomas (measured by the expression of CD86, HLA-DR, CD163, and LYZ) suggesting that IDH status and treatment had a minimal impact on DC activation (Supplementary Figure 3Q and R).

Antigen presentation function is linked to glioma-associated MG.<sup>19</sup> However, a direct comparison of antigen-presenting potential among professional APC-like DCs is

lacking. We used our transcriptomic data to derive an APC score comprising major histocompatibility complex (MHC) class I and class II-associated gene modules and compared putative APC-like cells with cDC1 and cDC2. All professional APCs (cDC1, cDC2, and Mreg-DC) showed similar APC scores ([Supplementary Figure 3S](#) and [T; Supplementary Table 12](#)). Among the MG subpopulations, MG\_APC-like clusters 1 and 2 showed higher antigen-presenting potential than did the other MG clusters; however, the scores were lower than that of cDCs. Other MDM and MAC clusters showed antigen-presenting potential comparable to those of cDC1 and cDC2 ([Supplementary Figure 3T](#)). To confirm this hypothesis, we utilized our spectral cytometric data and derived APC scores from B2M (MHC class I), HLA-DR (MHC class II), CD86 and LYZ, which were used to compare APC cell types across gliomas. While MG and Mo exhibited higher APC scores in IDH-wt gliomas than in IDH-mut gliomas, scores of MDM clusters increased with disease recurrence ([Figure 3L; Supplementary Figure 3U](#)). These results suggested that APC contributes to the inflammatory milieu in gliomas. Therefore, canonical inflammatory (eg, *IL1B* and *TNF*) and immunoregulatory (eg, *IL10* and *TGFB1*) genes were used to derive inflammatory and immunoregulatory scores, respectively ([Supplementary Table 13](#)), to assess the proinflammatory and anti-inflammatory effects mediated by myeloid cells in the glioma TIME. MG/MG-like cells exhibited inflammatory scores higher than immunoregulatory scores across gliomas ([Supplementary Figure 3V](#) and [X](#)).

### Characterization of Infiltrating T and NK Cell Subsets in the Glioma TIME

Unsupervised clustering analysis revealed 6 CD4 T and 9 CD8 T lymphocyte clusters ([Supplementary Figure 4A; Figure 4A](#)). Glioma-associated CD4 T cell subpopulations comprised CD4<sup>+</sup> ANXA1<sup>+</sup> CD4 T\_Annexin 1, SELL<sup>+</sup> CD4 T\_Naive, CST7<sup>+</sup> CD4 T\_Cytotoxic, FOXP3<sup>+</sup> Tregs, and *BCL6*-expressing T-follicular helper (Tfh) cells ([Supplementary Figure 4B; Supplementary Table 14](#)). Along with leukocyte activation and adhesion GO terms seen across clusters, CD4 T\_Annexin 1 was also associated with metabolic GO terms such as cellular response to corticosteroids and glucocorticoids ([Supplementary Figure 4C; Supplementary Table 15](#)). Spectral cytometry analyses revealed comparable proportions of activated and effector Ki-67<sup>+</sup>, GNLY<sup>+</sup>, Granzyme B (GZMB<sup>+</sup>), and GZMB<sup>+</sup>GNLY<sup>+</sup> CD4<sup>+</sup> T subpopulations across glioma subtypes suggesting similar activities of CD4<sup>+</sup> T cell activity ([Supplementary Figure 4D](#)).

Similarly, effector CD8 T lymphocytes were defined as *LEF1*<sup>+</sup> CD8 T\_Effector Memory and *IL7R*<sup>+</sup> CD8 T\_Effector 1 using DEGs and GO terms. In addition, we observed GZMH<sup>+</sup> CD8 T\_Effector 2 displaying central memory T cell-like signature (SELL, *IL7R*, and *CCR7*), and CD8 T\_Cytotoxic lymphocytes expressing multiple tumorcidal molecules such as *IFNG*, *TNF*, GZMB, GNLY, and *PRF1* ([Figure 4A; Supplementary Figure 4E and F; Supplementary Tables 16 and 17](#)). Comparison of cytotoxic molecules across gliomas revealed that the granzyme family of proteins (eg, encoded by *GZMA* and *GZMK*) was more abundant than *PRF1* and *GNLY* ([Supplementary Figure 4G](#)). Spectral

cytometric analyses confirmed the abundance of GZMB in comparison to those of PRF1 and GNLY-expressing CD8<sup>+</sup> T cells across gliomas. Specifically, higher proportions of activated Ki-67<sup>+</sup> and GZMB<sup>+</sup> CD8<sup>+</sup> T lymphocytes were observed in IDH-wt gliomas than in IDH-mut gliomas, whereas the proportions of GNLY<sup>+</sup>, GZMB<sup>+</sup>, GZMB<sup>+</sup>GNLY<sup>+</sup>, and GZMB<sup>+</sup>GNLY<sup>+</sup>PRF1<sup>+</sup> cytotoxic CD8<sup>+</sup> T lymphocyte subsets were similar across glioma subtypes ([Figure 4B; Supplementary Figure 4H](#)). Among the co-inhibitory molecules, *HAVCR2* and *CTLA4* expression were restricted to the CD8 T innate-like cluster. In contrast, *LAG3* and *TIGIT* were expressed across all CD8 T cell clusters, and *PDCD1* expression was lowest in these clusters ([Supplementary Figure 4I; Supplementary Table 18](#)).

The heterogeneity of NK cells has been described in the blood and spleen of healthy humans at single-cell resolution<sup>43–46</sup> and 2 distinct NK cell subpopulations, immature CD56<sup>bright</sup> CD16<sup>−</sup> and a highly cytotoxic CD56<sup>int</sup> CD16<sup>+</sup> have been documented in IDH-wt gliomas and brain metastasis, respectively.<sup>20</sup> Our scRNA-seq analyses revealed 5 NK cell subpopulations including an *IL32* and *CD8A*-expressing NK-like CD8 cluster and an *FCGR3A* encoding CD16<sup>+</sup> NK\_cytotoxic cluster highly expressing *GNLY*, GZMB, and *PRF1*. In addition, we identified a *B3GNT7*- and *CEBPD*-expressing NK\_inflammatory cluster with GO term associated with response to glucocorticoid and a CD56<sup>hi</sup> NK\_hsp cluster (*HSPA1A* and *HSPA6*). The CD56<sup>hi</sup> NK\_IFN cluster was associated with the expression of interferon-stimulated genes (ISGs; *IFITM2*, and *IL18*) ([Figure 4C; Supplementary Figure 4J and K; Supplementary Tables 19 and 20](#)). NK cells showed similar proliferation, activation, and cytotoxic phenotypes in gliomas ([Figure 4D; Supplementary Figure 4L](#)).

### Identification of Rare Unconventional Innate T Cells in the Glioma TIME

Although rare innate T cell populations such as intraepithelial innate lymphoid-like cells have been reported in the glioma TIME of humans,<sup>20</sup> other such rare cell types have not been extensively investigated. We confirmed the presence of TCR- $\gamma\delta$  cells and found that their cytotoxic status was similar across all gliomas ([Supplementary Figure 4M](#)). Additionally, rare innate T cells in our scRNA-seq discovery dataset were confirmed using canonical protein markers ([Supplementary Figure 2K](#)). This analysis revealed an abundance of glycolipid antigen-sensing Ki-67<sup>+</sup> proliferative natural killer T (NKT) cells in the IDH-wt group compared to that in NGB group. However, the proportion of cytotoxic NKT cells, as determined by GZMB and GNLY expression was comparable across gliomas ([Figure 4E](#)). Interestingly, MAIT-like cells have been identified by genomic analyses in GBM,<sup>15</sup> however, they have not been confirmed using the expression of MAIT-specific canonical protein markers. Our study confirmed the presence of TCR- $\alpha$ V7.2<sup>+</sup> MAIT cells across gliomas by spectral cytometric analysis. Comparable activation (Ki-67) and cytotoxic status (GZMB and GNLY) of MAIT cells were observed across gliomas ([Figure 4F](#)).

Interestingly, as reported for primary IDH-wt gliomas of humans, B-lineage cells coexisted with Tfh cells in the glioma TIME as immature B cells (*IGHD*) and

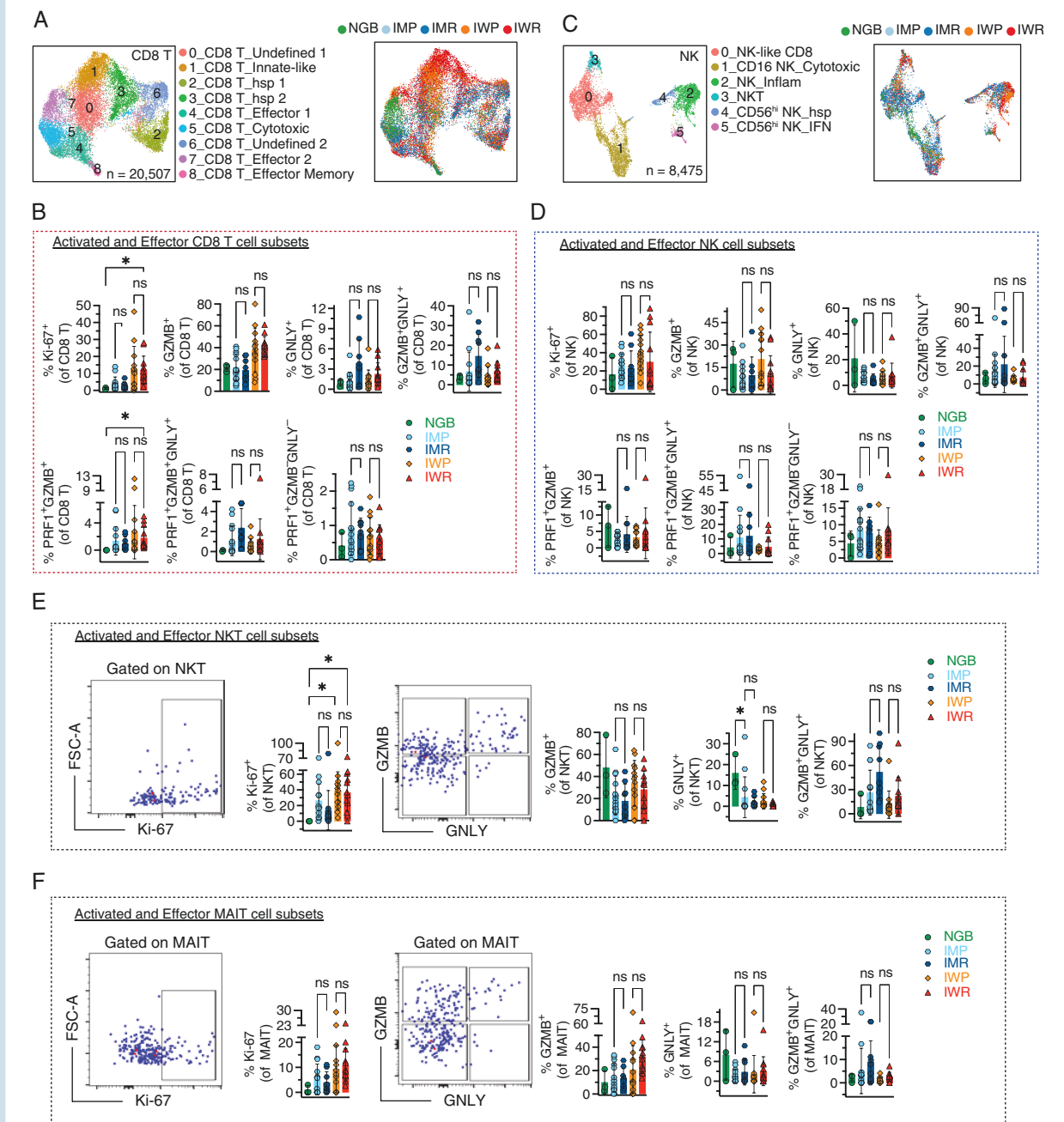


**Figure 4.** Diversity of glioma-associated cytotoxic lymphoid cells. (A) UMAP visualization of unsupervised clustering analysis of CD8 T cell clusters defined by scRNA-seq. Cells are color-coded for their inferred CD8 T lymphocyte subpopulations (left) and the glioma subtypes of their corresponding tumors (right). (B) Color-coded scatter bar plots represent the proportions of activated and effector CD8 T cell subsets as defined by Ki-67<sup>+</sup>, GZMB<sup>+</sup>, GNLY<sup>+</sup>, and GZMB<sup>+</sup>GNLY<sup>+</sup> cells (top panels), and PRF1<sup>+</sup>GZMB<sup>+</sup>, PRF1<sup>+</sup>GZMB<sup>+</sup>GNLY<sup>+</sup> and PRF1<sup>+</sup>GZMB<sup>-</sup>GNLY<sup>-</sup> (bottom panels) cells. (C) UMAP visualization of unsupervised clustering analysis of NK cell clusters defined by scRNA-seq. Cells are color-coded for their inferred NK cell subpopulations (left), and the glioma subtypes of their corresponding tumors (right). (D) Color-coded scatter bar plots represent the proportions of activated and effector NK cell subsets as defined by Ki-67<sup>+</sup>, GZMB<sup>+</sup>, GNLY<sup>+</sup>, and GZMB<sup>+</sup>GNLY<sup>+</sup> cells (top panels), and PRF1<sup>+</sup>GZMB<sup>+</sup>, PRF1<sup>+</sup>GZMB<sup>+</sup>GNLY<sup>+</sup>, and PRF1<sup>+</sup>GZMB<sup>-</sup>GNLY<sup>-</sup> cells (bottom panels) expression. (E) Pseudo-color FCM plots showing the expression of Ki-67, GZMB, and GNLY on NKT cells, and corresponding color-coded scatter bar plots represent the proportions of activated and effector NKT cell subsets as defined by Ki-67<sup>+</sup>, GZMB<sup>+</sup>, GNLY<sup>+</sup>, and GZMB<sup>+</sup>GNLY<sup>+</sup> cells. (F) Pseudo-color FCM plots showing the expression of Ki-67, GZMB, and GNLY on MAIT cells, and corresponding color-coded scatter bar plots represent the proportions of activated and effector MAIT cell subsets as defined by Ki-67<sup>+</sup>, GZMB<sup>+</sup>, GNLY<sup>+</sup>, and GZMB<sup>+</sup>GNLY<sup>+</sup> cells. Statistical significance in B, D, E, and F was determined by using the Kruskal-Wallis test at \* $P < .05$ , \*\* $P < .01$ , and \*\*\* $P < .001$  between NGB and glioma subtypes, IMP versus IMR, IWP versus IWR, and IMP versus IWP; n.s. = not significant. Glioma subtypes used for spectral cytometry analysis: NGB ( $n = 3$ ), IMP ( $n = 14$ ), IMR ( $n = 9$ ), IWP ( $n = 13$ ), and IWR ( $n = 12$ ).

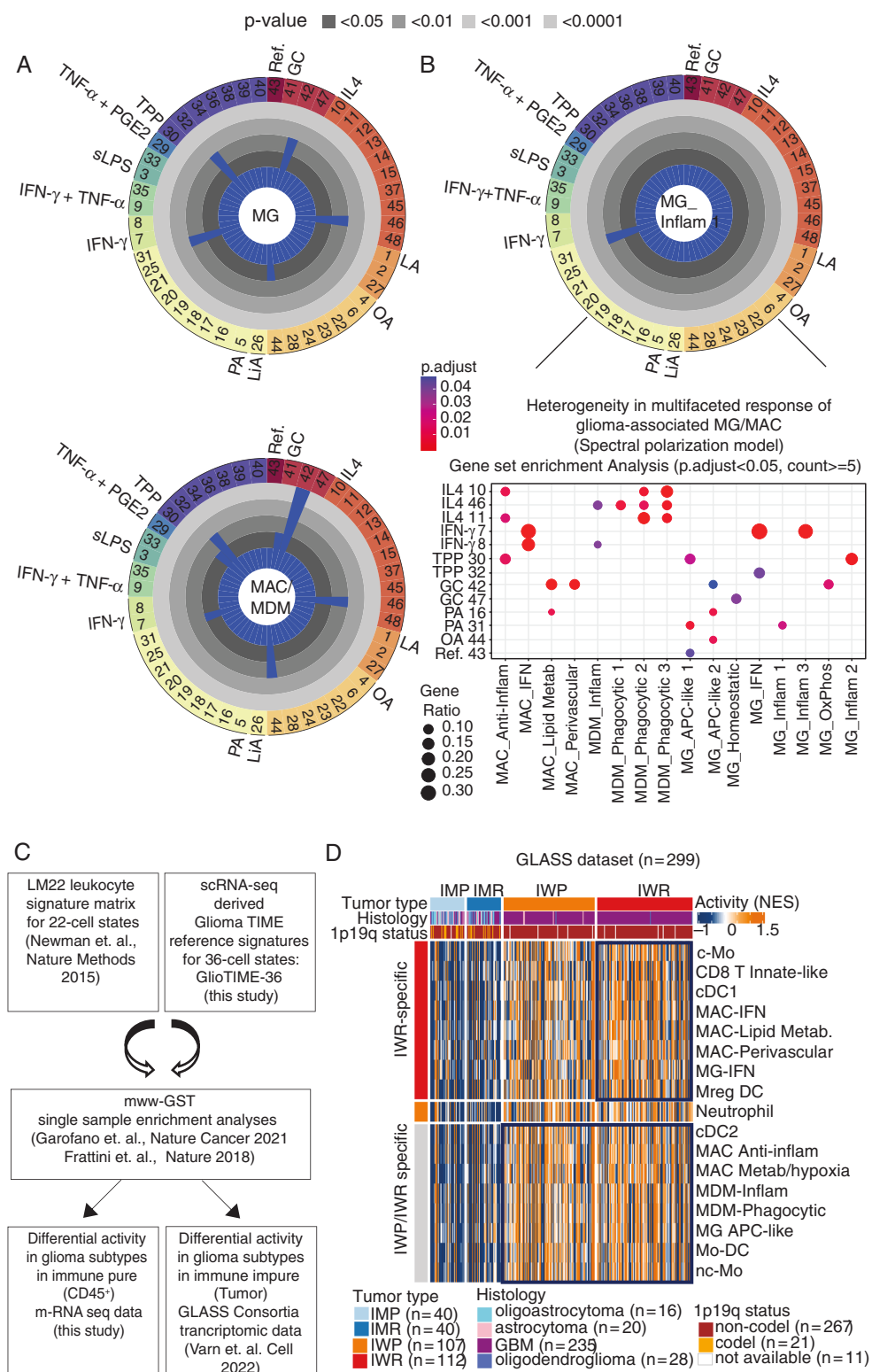
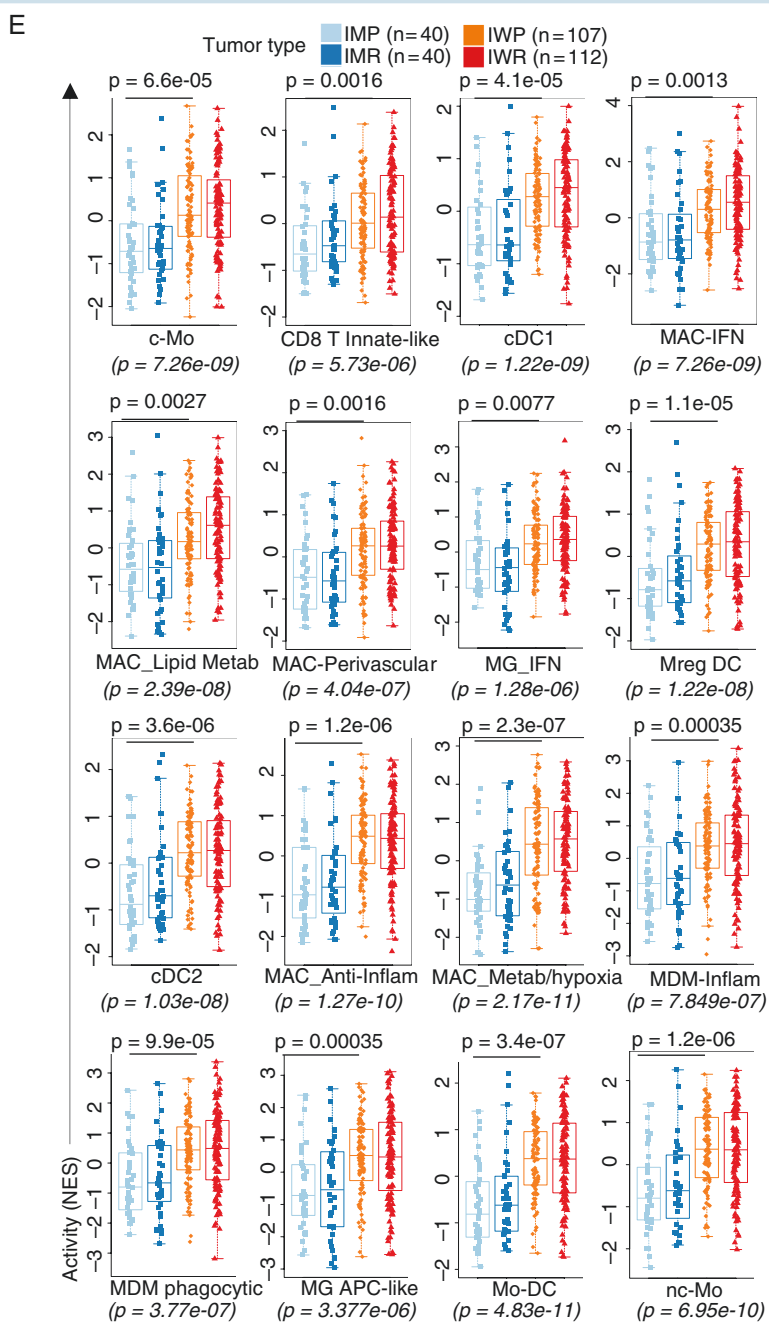


**Figure 5.** Transcriptomic utility signatures defined by scRNA-seq for characterizing spectral polarization modules of glioma-associated MG/MAC and defining GlioTIME-36 gene signatures to infer leukocyte abundance. (A) Circos plot showing overrepresented stimulus-specific polarization gene expression modules for MG (upper) and MAC/MDM (lower) as pseudo-bulk versus respective multispectral macrophage polarization references. Bar heights and color indicate statistical significance ( $P < .05$ –.0001). Gene expression modules are represented as glucocorticoid (GC), interferon-gamma (IFN- $\gamma$ ), lauric acid (LA), linoleic acid (LiA), oleic acid (OA), palmitic acid (PA), prostaglandin E2 (PGE2), standard lipopolysaccharide (sLPS), tumor necrosis alpha (TNF- $\alpha$ ), TPP (TNF- $\alpha$  + PGE2 + Pam3CysSerLys4), and interleukin-4 (IL-4). (B) Circos plot (upper panel)



showing overrepresented stimulus-specific polarization gene expression modules for MG cluster (MG\_inflam 1) defined by scRNA-seq versus respective multispectral macrophage polarization references. Bubble plot (lower panel) showing gene set enrichment analysis of MG and MAC/MDM subsets against stimulus-specific polarization gene expression modules. Each bubble represents a gene expression module. Bubble size corresponds to gene ratio, and color indicates statistical significance. Only modules with  $\geq 5$  overlapping genes and an adjusted  $P$ -value  $< .05$  are shown here. (C) A schematic of calculating the normalized enrichment score (NES) of the GlioTIME-36 and LM22 signatures derived from bulk mRNA-seq datasets of CD45<sup>+</sup> leukocytes (immune pure) from glioma subtypes; NGB ( $n = 1$ ), IMP ( $n = 3$ ), IMR ( $n = 4$ ), IWP ( $n = 3$ ), and IWR ( $n = 4$ ), and GLASS dataset ( $n = 299$ ). (D) Heatmap of GlioTIME-36 with differential NES activity in different glioma subtypes. Statistical significance was determined using the MWU test at  $P < .05$  and effect size  $> 0.3$ . The top annotation tracks define glioma subtypes, histology, and 1p 19q codeletion status. (E) Box plots represent the mean NES  $\pm$  SD of indicated tumor-associated leukocyte subpopulation across glioma subtypes inferred from the GlioTIME-36 signatures in the GLASS dataset.  $P$ -values derived by the Kruskal-Wallis  $H$  test are shown on the x axis.  $P$ -values on the top were derived from post hoc correction by Nemenyi's test for multiple subgroups comparison of continuous variables.

antibody-producing plasma cells (*IGHM*, *IGLC2*, and *IGHA1*), albeit as a rare infiltrating subpopulation (Supplementary Figure 4N). In summary, we provide a detailed overview of several cytotoxic lymphoid phenotypes that may contribute to glioma immunity (Supplementary Figure 4O; Supplementary Table 21).

### Spectral Polarization of Glioma-Associated Myeloid Cells

Tissue macrophages exhibit multifaceted polarization in response to microenvironmental cues; therefore, we evaluated the polarization continuum of MG with 9 distinct programs of macrophage activation as previously described.<sup>16</sup> Recent bulk RNA-seq analysis has pointed to multifaceted polarization of tumor-associated MG and MDMs.<sup>21</sup> To recapitulate this observation, we generated a pseudo-bulk dataset derived from MG and MAC/MDM clusters of our scRNA-seq datasets and subjected them to similar gene set enrichment analyses. This analysis showed a multifaceted polarization pattern in both MG and MAC/MDM as previously shown (Figure 5A). However, when scRNA-seq data from discrete clusters were used, a variety of polarization states restricted to mostly 1 or 2 modules were observed (Figure 5B; Supplementary Table 22). This included the widely studied proinflammatory modules (MAC\_IFN, MDM\_Inflam, MG\_IFN, and MG\_Inflam 3) and a polarization state associated with chronic inflammatory stimuli (MAC\_Anti-inflam, MAC\_APC-like 1, and MG\_Inflam 2). Additionally, we identified several MAC/MDM clusters associated with an anti-inflammatory polarization module (MDM\_Phagocytic 1–3). We observed MG/MAC clusters that spanned metabolic states responsive to glucocorticoid (GC, MG\_Perivascular, Mac\_Perivascular, and MG\_OxPhos), and palmitic acid (PA, MG\_Inflam 1). Interestingly, MG\_APC-like 2 shared polarizations across oleic acid (OA), PA and GC responsive states. We also observed TPP and PA co-responsive states associated with MG\_APC like 1 (Figure 5B; Supplementary Table 22). Since dexamethasone is routinely administered as a synthetic GC to suppress glioma-associated inflammation,<sup>47</sup> and can result in GC responsive states,<sup>14</sup> we hypothesized that GC-polarized MG/MAC states are a result of dexamethasone treatment. We observed that GC-polarized MG/MAC states were present even in the IMP sc-RNA-seq cohort, which did not receive dexamethasone prior to surgery, suggesting glioma milieu driven polarization. Similar polarization states have been previously documented, even in recurrent GBMs.<sup>14</sup> Overall, we provide extensive clarification of the myeloid cell states and their associated polarization spectra.

### Defining Glioma-Specific Immune Gene Signatures for Deconvoluting Immune Cells

Next, we utilized our glioma TIME-specific 36 cell-state (Supplementary Table 23) signatures (termed GlioTIME-36) for deconvolution<sup>48,49</sup> and bulk RNA-seq of purified CD45<sup>+</sup> leukocytes from a subset of glioma samples used in this study (Supplementary Figure 5A). This analysis recapitulated the immune contexture as inferred by scRNA-seq (for instance, reduction of MG and abundance of T cells in IWR, Supplementary Figure 5A). We also found that the CD45<sup>lo</sup>

fraction was enriched for MG, whereas CD45<sup>hi</sup> was mostly composed of lymphoid cells. The Glioma Longitudinal AnalySiS consortium dataset<sup>50</sup> was chosen for deconvolution as it mirrored the glioma pathologies used in this study (Figure 5C and D; Supplementary Figure 5B and C). When compared to LM22,<sup>51</sup> a previously defined signature lacking information about the most abundant cell type MG and rare cell types discovered in our study, GlioTIME-36 provided a realistic representation of immune contexture of glioma (Supplementary Figure 5B and C). Additionally, we observed differential abundance of several cell states (eg, MG\_Inflammatory, MG\_APC-like, Mo-DC, and MAIT) among the glioma subtypes, which were consistent with the findings of spectral cytometry (Figure 5E; Supplementary Figure 5D), thereby providing a refined framework for clinical immunogenomic interpretation of glioma datasets.

## Discussion

This study provides a large immunophenotyping resource for CD45<sup>+</sup> leukocytes from human adult gliomas with approximately 146 000 cells probed using scRNA-seq, and more than 2 million cells analyzed using spectral cytometry. Our systematic analyses of treatment-naïve and relapsed IDH-mut and IDH-wt gliomas provide a framework for delineating glioma immune contexture and suggest that treatment paradigms and IDH status contribute to the differences among glioma TIME. Inflammation-associated with glioma relapse and surgical and chemoradiation interventions together contributed to decreased proportions of MG cells in recurrent gliomas irrespective of IDH status. Radiation-induced transient proliferation of MG followed by long-term inflammation-induced apoptosis has been previously observed.<sup>52,53</sup> Therefore, we speculate that the reduction in MG population could be a consequence of a combination of treatment effects and pathology-induced chronic inflammation, a postulate that is being investigated in ongoing studies in our laboratory. In contrast, residual MG gained inflammatory and proliferative signatures in IDH-wt gliomas, suggesting remodeling of these cells in response to alterations in the tumor microenvironment. Our transcriptomic findings suggest that MG and other myeloid cell clusters manifest a putative proinflammatory rather than an anti-inflammatory milieu characterized by the expression of *TNF*, *IL1B*, *SPP1*, and other cytokine genes. Based on these observations, we identified novel inflammatory MG subpopulations, defined by TREM2 and GNLY co-expression, which were proportionately abundant in the IWR glioma subtype. Intriguingly, MG expresses GNLY, a cytotoxic molecule restricted to lymphoid cells.<sup>54</sup> GNLY can function as an immune alarmin to recruit and activate APC-like myeloid cells,<sup>55</sup> which is a plausible testable hypothesis owing to the correlative abundance of several APCs (eg, MDMs and DCs) and GNLY<sup>+</sup> MG in IDH-wt gliomas. Prior studies may have missed GNLY<sup>+</sup> MG owing to the rarity of these populations and lack of a murine homolog.<sup>56</sup>

Monocytic infiltrates in the brain can acquire characteristics like those of tissue myeloid cells, and we provide cytometry-based evidence of monocytic derivatives of MG (CCR2<sup>+</sup> Mo-MG) and DCs (Mo-cDC1 and Mo-cDC2) in the

glioma TIME. Notably, the MG and MDM subpopulations abundantly expressed both MHC class I (eg, *B2M*) and class II (eg, *CD74*) genes in IDH-wt tumors, indicating their putative APC-like characteristics. While APCs and phagocytic strength of MG were enhanced in IDH-wt gliomas, MDMs gained these properties upon glioma relapse. In conjunction with previous reports showing that MG and MDMs are linked to APC-like cross-presentation functions,<sup>57,58</sup> our study showed enhanced number of APCs and phagocytic strength of MG in IDH-wt gliomas, whereas MDMs gained these properties upon glioma relapse. Additionally, we identified GNLY-expressing inflammatory MG subpopulations in the gliomaTIME. Altogether, this evidence indicates inflammatory imprinting of myeloid cells by the tumor microenvironment, particularly in IDH-wt gliomas.

Glioma infiltrative T cells exhibited comparable cytotoxic phenotypes across tumor pathologies and are mostly driven by *GZMA*, *GZMK*, and *CST7* expression, as previously reported,<sup>13</sup> and we observed a subset of these cytotoxic phenotypes (*GZMB*, *PRF1*, and *GNLY*) by cytometry investigation. In addition to T lymphocytes, we report other cytotoxic lymphocytes comprising heterogeneous NK cell subpopulations, NKT, and MAIT cells as newly identified contributors to glioma immunity. Notably, a subset of inflammatory NK cells abundantly expressed *CEBP* family genes, which coexisted with CD56<sup>hi</sup> NK cells expressing IFN-associated gene signatures and CD16<sup>hi</sup> NK cells. Overall, the cytotoxic status of NK cells remained comparable across treatment-naïve and relapsed IDH-wt and IDH-mutant gliomas suggesting that disease relapse or IDH status did not affect NK cell-mediated tumoricidal activity.

Finally, we leveraged the advanced understanding of the glioma TIME to address the much-needed reference gene signatures beyond LM22. To this end, we provide a unique reference of GlioTIME-36 for immunogenomics deconvolution of immune pure and tumor impure bulk genomics datasets exemplifying their utility with the GLASS transcriptomics dataset. Our study also clarifies that rather than being multifaceted, macrophages exhibit heterogeneous polarization states spanning proinflammatory and anti-inflammatory, as well as lipid and metabolic modules.

The findings in this study provide a robust consolidated dataset of the glioma TIME with limitations that are characteristic of such study designs. Although the number of patients per glioma subtype was limited in this study, sufficiently large number of cells were sampled per patient to curate a high-quality discovery dataset. Notably, extrapolation to glioma subtype-specific associations should not be derived exclusively from our transcriptome data, but rather from the statistically significant and spectral cytometry-validated findings in this study. Our findings suggest that glioma-associated myeloid cells may be inflammatory. Certain MG and MDM cell states with APC-like potential and macrophage polarization beyond proinflammatory and anti-inflammatory phenotypes require additional vetting by *in situ*, *in vitro*, and *ex vivo* functional immunoassays. In summary, we provide a reliable resource of the glioma TIME, which can be used to uncover actionable targets for immunotherapy in brain cancers.

## Supplementary material

Supplementary material is available online at *Neuro-Oncology* (<https://academic.oup.com/neuro-oncology>).

## Keywords

glioma | isocitrate dehydrogenase | microglia | tumor immune microenvironment

## Funding

This study was supported by generous philanthropic contributions from The University of Texas (UT) MD Anderson Cancer Center (MDACC) Moon Shots Program, Marnie Rose Foundation, and NIH grants R21 CA222992 and R01CA225963. This study was partly supported by the UT MDACC start-up research fund to L.W. and CPRIT Single Core grant RP180684 to N. E. N. We thank the UT MDACC Odyssey fellowship programs for their generous training and fellowship support to P.G. We would like to thank Haidee D. Chancoco for her contribution to RNA isolation for bulk mRNA-seq at the Biospecimen Extraction Resource of the MD Anderson Cancer Center, Advanced Technology Genomics Core supported by NCI grant CA016672 for library preparation and sequencing, and David W. Dwyer and Karen C. Dwyer at the Advanced Cytometry and Sorting Core Facility supported by NCI P30 CA016672.

## Conflict of interest statement

All authors declare no competing interests except H.S., S.A.S., E.R.P.C., and A.B.H. H.S. is a founder of NextGen Omics. S.A.S is engaged in consulting with Boston Scientific, Neuropace, Zimmer Biomet, Koh Young, Sensoria Therapeutics, and Varian Medical. E.R.P.C. executed consulting assignments for Nuclei Lt, iTeos Belgium. A.B.H. has engaged in contracts with Abbvie, Ainylam, Codiak, Cellularity and received royalties from DNATrix, Celldex Therapeutics and consulting fees from Novocure, Istari Oncology, Alphasights, and BlueRock Therapeutics. A.B.H. is an advisory board member with WCG Oncology, Caris Life Science, Children's National Hospital Brain Tumor Institute, UCSF Neurological and Brain Tumor Program, Dana Farber and Brigham and Women's Hospital (P01), Cleveland Clinic Sex Difference (P01), UCLA Brain SPORE, National Cancer Advisory Board. She has stocks in Caris Life Sciences and is a recipient of gifts and other services from Moleculin, Carthera, and Takeda.

## Acknowledgments

We thank Alicia Goldman, Cynthia Kassab, and Martina Ott for their contributions to tissue logistics in the scRNA-seq pipelines.

In part, the patient specimens analyzed with spectral cytometry in this study were contributed by CNS tumor Analysis Stream (CATALYST) program at UT MDACC and we extend our gratitude to entire CATALYST team and especially Douglas Neilsen for clinical evaluation for specimens used in this study. We thank Sanaalarab Al-Enazy for providing the schematic illustration.

Netherlands Cancer Institute, Amsterdam, the Netherlands (H.S.); Department of Neurosurgery, Baylor College of Medicine, Houston, Texas, USA (S.A.S.); Department of Neurology and Neuroscience, Baylor College of Medicine, Houston, Texas, USA (A.M.); Department of Neurosurgery, Northwestern University, Evanston, Illinois, USA (A.B.H.); MD Anderson UTHealth Graduate School of Biomedical Sciences, Houston, Texas, USA (M.P., N.E.N., L.W., K.P.B.)

## Authorship statement

Conception and design of the study: P.G. and K.P.B. Acquisition of glioma samples and processing: P.G., S.O., M.P., N.M., A.A., J.G., and K.B. Acquisition of epileptic clinical specimens: S.A.S. and A.M. Accessing clinical information of patients with glioma: C.K.M. Sample preparation for scRNA-seq and bulk RNA-seq: P.G. and K.B. Spectral cytometry and data analysis: P.G., S.O., and K.C.D. Leukocyte preparation: M.P. and N.M. scRNA-seq experiments: T.M.T. and J.L. Design of cytometry panel: K.C.D. and P.G. CODEX assay: R.S., S.B., P.G., K.B., and E.R.P.C. Spectral cytometry experiments and analysis: P.G., S.O., K.C.D., K.C., and S.O. scRNA-seq and bulk mRNA-seq analysis: M.D., L.W., and P.G. Spectral cytometry correlation analyses: K.P.B., H.S., and R.T. Constructive comments: F.F.L., N.E.N., and A.B.H. GLASS dataset analyses: S.M., A.I., P.G., K.P.B., P.G., M.D., L.W., and K.P.B. Interpretation of scRNA-seq data: S.M. Interpretation of spectral cytometry data: P.G., K.C.D., and K.P.B. Draft manuscript preparation: P.G., M.D., L.W., and K.P.B. Proofreading: P.G., R.T., and K.P.B.

## Data and code availability

The processed scRNA-seq and bulk RNA-seq generated in this study are publicly available with unrestricted access through the GSE22522 reference super series upon request. All other data and code available upon request.

## Affiliations

Department of Translational Molecular Pathology, The University of Texas MD Anderson Cancer Center, Houston, Texas, USA (P.G., S.O., R.T., G.K., M.P., N.M., A.A., K.B., R.S., S.B., E.R.P.C., K.P.B.); Department of Genomic Medicine, The University of Texas MD Anderson Cancer Center, Houston, Texas, USA (M.D., L.W.); Department of Systems Biology, The University of Texas MD Anderson Cancer Center, Houston, Texas, USA (T.M.T., J.L., N.E.N.); Department of Neurosurgery, The University of Texas MD Anderson Cancer Center, Houston, Texas, USA (J.G., B.P.K., F.F.L., K.P.B.); Department of Neuro-Oncology, The University of Texas MD Anderson Cancer Center, Houston, Texas, USA (C.K.M.); Department of Pathology, The University of Texas MD Anderson Cancer Center, Houston, Texas, USA (J.H.); Department of Hematopoietic Biology and Malignancy, The University of Texas MD Anderson Cancer Center, Houston, Texas, USA (K.C., K.C.D.); Department of Neurological Surgery, Sylvester Comprehensive Cancer Center, University of Miami Miller School of Medicine, Miami, Florida, USA (S.M., A.I.);

## References

- Spiteri AG, Wishart CL, Pamphlett R, Locatelli G, King NJC. Microglia and monocytes in inflammatory CNS disease: integrating phenotype and function. *Acta Neuropathol.* 2022;143(2):179–224.
- Leng F, Edison P. Neuroinflammation and microglial activation in Alzheimer disease: where do we go from here? *Nat Rev Neurol.* 2021;17(3):157–172.
- Buonfiglioli A, Hambardzumyan D. Macrophages and microglia: the cerberus of glioblastoma. *Acta Neuropathol Commun.* 2021;9(1):54.
- Lavin Y, Winter D, Blecher-Gonen R, et al. Tissue-resident macrophage enhancer landscapes are shaped by the local microenvironment. *Cell.* 2014;159(6):1312–1326.
- Nagarsheth N, Wicha MS, Zou W. Chemokines in the cancer microenvironment and their relevance in cancer immunotherapy. *Nat Rev Immunol.* 2017;17(9):559–572.
- Ohgaki H, Kleihues P. The definition of primary and secondary glioblastoma. *Clin Cancer Res.* 2013;19(4):764–772.
- Balentova S, Adamkov M. Molecular, cellular and functional effects of radiation-induced brain injury: a review. *Int J Mol Sci.* 2015;16(11):27796–27815.
- Deeken JF, Löscher W. The blood-brain barrier and cancer: transporters, treatment, and Trojan horses. *Clin Cancer Res.* 2007;13(6):1663–1674.
- Karachi A, Dastmalchi F, Mitchell DA, Rahman M. Temozolomide for immunomodulation in the treatment of glioblastoma. *Neuro Oncol.* 2018;20(12):1566–1572.
- Yeo AT, Rawal S, Delcuze B, et al. Single-cell RNA sequencing reveals evolution of immune landscape during glioblastoma progression. *Nat Immunol.* 2022;23(6):971–984.
- Wei J, Chen P, Gupta P, et al. Immune biology of glioma associated macrophages and microglia: functional and therapeutic implications. *Neuro Oncol.* 2019;22(2):noz212.
- Lee AH, Sun L, Mochizuki AY, et al. Neoadjuvant PD-1 blockade induces T cell and cDC1 activation but fails to overcome the immunosuppressive tumor associated macrophages in recurrent glioblastoma. *Nat Commun.* 2021;12(1):6938.
- Mathewson ND, Ashenberg O, Tirosh I, et al. Inhibitory CD161 receptor identified in glioma-infiltrating T cells by single-cell analysis. *Cell.* 2021;184(5):1281–1298.e26.
- Pombo Antunes AR, Scheyltjens I, Lodi F, et al. Single-cell profiling of myeloid cells in glioblastoma across species and disease stage reveals macrophage competition and specialization. *Nat Neurosci.* 2021;24(4):595–610.
- Ravi VM, Neidert N, Will P, et al. T-cell dysfunction in the glioblastoma microenvironment is mediated by myeloid cells releasing interleukin-10. *Nat Commun.* 2022;13(1):925.
- Xue J, Schmidt SV, Sander J, et al. Transcriptome-based network analysis reveals a spectrum model of human macrophage activation. *Immunity.* 2014;40(2):274–288.

17. Hambardzumyan D, Gutmann DH, Kettenmann H. The role of microglia and macrophages in glioma maintenance and progression. *Nat Neurosci*. 2016;19(1):20–27.
18. Murray PJ, Allen JE, Biswas SK, et al. Macrophage activation and polarization: nomenclature and experimental guidelines. *Immunity*. 2014;41(1):14–20.
19. Sankowski R, Böttcher C, Masuda T, et al. Mapping microglia states in the human brain through the integration of high-dimensional techniques. *Nat Neurosci*. 2019;22(12):2098–2110.
20. Friebel E, Kapolou K, Unger S, et al. Single-cell mapping of human brain cancer reveals tumor-specific instruction of tissue-invading leukocytes. *Cell*. 2020;181(7):1626–1642.e20.
21. Klemm F, Maas RR, Bowman RL, et al. Interrogation of the microenvironmental landscape in brain tumors reveals disease-specific alterations of immune cells. *Cell*. 2020;181(7):1643–1660.e17.
22. Abdelfattah N, Kumar P, Wang C, et al. Single-cell analysis of human glioma and immune cells identifies S100A4 as an immunotherapy target. *Nat Commun*. 2022;13(1):767.
23. Ruiz-Moreno C, Salas SM, Samuelsson E, et al. Harmonized single-cell landscape, intercellular crosstalk and tumor architecture of glioblastoma. *bioRxiv*. 2022.
24. Zamler DB, Shingu T, Kahn LM, et al. Immune landscape of a genetically engineered murine model of glioma compared with human glioma. *JCI Insight*. 2022;7(12):e148990.
25. Friedrich M, Sankowski R, Bunse L, et al. Tryptophan metabolism drives dynamic immunosuppressive myeloid states in IDH-mutant gliomas. *Nat Cancer*. 2021;2(7):723–740.
26. McGranahan T, Therkelsen KE, Ahmad S, Nagpal S. Current state of immunotherapy for treatment of glioblastoma. *Curr Treat Options Oncol*. 2019;20(3):24.
27. Sheng J, Ruedl C, Karjalainen K. Most tissue-resident macrophages except microglia are derived from fetal hematopoietic stem cells. *Immunity*. 2015;43(2):382–393.
28. Hussain SF, Yang D, Suki D, et al. The role of human glioma-infiltrating microglia/macrophages in mediating antitumor immune responses. *Neuro Oncol*. 2006;8(3):261–279.
29. Bowman RL, Klemm F, Akkari L, et al. Macrophage ontogeny underlies differences in tumor-specific education in brain malignancies. *Cell Rep*. 2016;17(9):2445–2459.
30. Quail DF, Joyce JA. The microenvironmental landscape of brain tumors. *Cancer Cell*. 2017;31(3):326–341.
31. Adé K, Coronilla JS, Obino D, et al. Inflammation drives age-induced loss of tissue resident macrophages. *bioRxiv*. 2022.
32. Bajpai G, Schneider C, Wong N, et al. The human heart contains distinct macrophage subsets with divergent origins and functions. *Nat Med*. 2018;24(8):1234–1245.
33. Cronk JC, Filiano AJ, Louveau A, et al. Peripherally derived macrophages can engraft the brain independent of irradiation and maintain an identity distinct from microglia. *J Exp Med*. 2018;215(6):1627–1647.
34. Lai SM, Sheng J, Gupta P, et al. Organ-specific fate, recruitment, and refilling dynamics of tissue-resident macrophages during blood-stage malaria. *Cell Rep*. 2018;25(11):3099–3109.e3.
35. Cui Y, Wan Q. NKT cells in neurological diseases. *Front Cell Neurosci*. 2019;13(245).
36. Benmamar-Badel A, Owens T, Wlodarczyk A. Protective microglial subset in development, aging, and disease: lessons from transcriptomic studies. *Front Immunol*. 2020;11(430):430.
37. Masuda T, Sankowski R, Staszewski O, et al. Spatial and temporal heterogeneity of mouse and human microglia at single-cell resolution. *Nature*. 2019;566(7744):388–392.
38. Mathys H, Davila-Velderrain J, Peng Z, et al. Single-cell transcriptomic analysis of Alzheimer's disease. *Nature*. 2019;570(7761):332–337.
39. Kumar P, Lim A, Hazirah SN, et al. Single-cell transcriptomics and surface epitope detection in human brain epileptic lesions identifies pro-inflammatory signaling. *Nat Neurosci*. 2022;25(7):956–966.
40. Schulz D, Severin Y, Zanotelli VRT, Bodenmiller B. In-depth characterization of monocyte-derived macrophages using a mass cytometry-based phagocytosis assay. *Sci Rep*. 2019;9(1):1925.
41. Dutertre CA, Becht E, Irci SE, et al. Single-cell analysis of human mono-nuclear phagocytes reveals subset-defining markers and identifies circulating inflammatory dendritic cells. *Immunity*. 2019;51(3):573–589.e8.
42. Villani AC, Satija R, Reynolds G, et al. Single-cell RNA-seq reveals new types of human blood dendritic cells, monocytes, and progenitors. *Science*. 2017;356(6335):eaah4573.
43. Crinier A, Milpied P, Escalier B, et al. High-dimensional single-cell analysis identifies organ-specific signatures and conserved NK Cell subsets in humans and mice. *Immunity*. 2018;49(5):971–986.e5.
44. Sivori S, Vacca P, Del Zotto G, et al. Human NK cells: surface receptors, inhibitory checkpoints, and translational applications. *Cell Mol Immunol*. 2019;16(5):430–441.
45. Smith SL, Kennedy PR, Stacey KB, et al. Diversity of peripheral blood human NK cells identified by single-cell RNA sequencing. *Blood Adv*. 2020;4(7):1388–1406.
46. Yang C, Siebert JR, Burns R, et al. Heterogeneity of human bone marrow and blood natural killer cells defined by single-cell transcriptome. *Nat Commun*. 2019;10(1):1.
47. Swildens KX, Sillevius Smitt PAE, van den Bent MJ, French PJ, Geurts M. The effect of dexamethasone on the microenvironment and efficacy of checkpoint inhibitors in glioblastoma: a systematic review. *Neurooncol Adv*. 2022;4(1):vdac087.
48. Frattini V, Pagnotta SM, Tala, Fan JJ, et al. A metabolic function of FGFR3-TACC3 gene fusions in cancer. *Nature*. 2018;553(7687):222–227.
49. Garofano L, Migliozzi S, Oh YT, et al. Pathway-based classification of glioblastoma uncovers a mitochondrial subtype with therapeutic vulnerabilities. *Nat Cancer*. 2021;2(2):141–156.
50. Varn FS, Johnson KC, Martinek J, et al.; GLASS Consortium. Glioma progression is shaped by genetic evolution and microenvironment interactions. *Cell*. 2022;185(12):2184–2199.e16.
51. Chen B, Khodadoust MS, Liu CL, Newman AM, Alizadeh AA. Profiling tumor infiltrating immune cells with CIBERSORT. *Methods Mol Biol*. 2018;1711:243–259.
52. Han W, Umekawa T, Zhou K, et al. Cranial irradiation induces transient microglia accumulation, followed by long-lasting inflammation and loss of microglia. *Oncotarget*. 2016;7(50):82305–82323.
53. Leblond MM, Pérès EA, Helaine C, et al. M2 macrophages are more resistant than M1 macrophages following radiation therapy in the context of glioblastoma. *Oncotarget*. 2017;8(42):72597–72612.
54. Hsiao YW, Lai T-C, Lin Y-H, et al. Granulysin expressed in a humanized mouse model induces apoptotic cell death and suppresses tumorigenicity. *Oncotarget*. 2017;8(48):83495–83508.
55. Tewary P, Yang D, de la Rosa G, et al. Granulysin activates antigen-presenting cells through TLR4 and acts as an immune alarmin. *Blood*. 2010;116(18):3465–3474.
56. Huang LP, Lyu SC, Clayberger C, Krensky AM. Granulysin-mediated tumor rejection in transgenic mice. *J Immunol*. 2007;178(1):77–84.
57. Goddery EN, Fain CE, Lipovsky CG, et al. Microglia and perivascular macrophages act as antigen presenting cells to promote CD8 T cell infiltration of the brain. *Front Immunol*. 2021;12(726421):726421.
58. Muntjewerff EM, Meesters LD, van den Bogaart G, Revello NH. Antigen cross-presentation by macrophages. *Front Immunol*. 2020;11(1276):605958.